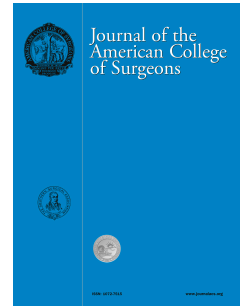# Journal Pre-proof

Imaging or a Fiber Probe-based Approach? Assessing Different Methods to Detect Near Infrared Autofluorescence for Intraoperative Parathyroid Identification

Giju Thomas, PhD, Malcolm H. Squires, MD, Tyler Metcalf, BS, Anita Mahadevan-Jansen, PhD, John E. Phay, MD, FACS

Please cite this article as: Thomas G, Squires MH, Metcalf T, Mahadevan-Jansen A, Phay JE, Imaging or a Fiber Probe-based Approach? Assessing Different Methods to Detect Near Infrared Autofluorescence for Intraoperative Parathyroid Identification, *Journal of the American College of Surgeons* (2019), doi: https://doi.org/10.1016/j.jamcollsurg.2019.09.003.

This is a PDF file of an article that has undergone enhancements after acceptance, such as the addition of a cover page and metadata, and formatting for readability, but it is not yet the definitive version of record. This version will undergo additional copyediting, typesetting and review before it is published in its final form, but we are providing this version to give early visibility of the article. Please note that, during the production process, errors may be discovered which could affect the content, and all legal disclaimers that apply to the journal pertain.

Imaging or a Fiber Probe-based Approach? Assessing Different Methods to Detect Near Infrared Autofluorescence for Intraoperative Parathyroid Identification

Giju Thomas[1,2], PhD, Malcolm H Squires[3], MD, Tyler Metcalf, BS[3], Anita Mahadevan-Jansen[1,2], PhD, John E Phay[3], MD, FACS

[1]Vanderbilt Biophotonics Center, Vanderbilt University, Nashville, TN 37235
[2]Department of Biomedical Engineering, Vanderbilt University, Nashville, TN 37235
[3]Division of Surgical Oncology, Ohio State University Comprehensive Cancer Center and Ohio State University Wexner Medical Center, 410 W 10th Ave, Columbus, OH 43210

Corresponding Author:

Dr. John E. Phay, MD, FACS
Professor of Surgery
Division of Surgical Oncology
Ohio State University Comprehensive Cancer Center and Ohio State University Wexner Medical Center
410 W 10th Ave
Columbus, OH 43210
Phone: (614) 293-8550
Fax: (614) 293-3465
Email address: john.phay@osumc.edu

Running Head: Near Infrared Autofluorescence for Parathyroid

Abstract

Background: Near infrared autofluorescence (NIRAF) can guide intraoperative parathyroid gland (PG) identification. NIRAF detection devices typically rely on imaging and fiber probe-based approaches. Imaging modalities provide NIRAF pictures on adjacent display monitors, while fiber probe-based systems measure tissue NIRAF and provide real-time quantitative information to objectively aid PG identification. Both device types recently gained FDA-approval for PG identification but have never been compared directly.

Methods: Patients undergoing thyroidectomy and/or parathyroidectomy were prospectively recruited. Target tissues were intraoperatively visualized with PDE-Neo II (imaging-based) and concurrently assessed with PTeye (fiber probe-based). For PDE-Neo II, NIRAF images were collected from *in situ* or excised tissues, alongside the surgeon's interpretation of visualized tissues, and retrospectively analyzed in a blinded fashion. The PTeye was concomitantly used to record NIRAF intensities and ratios from the same tissues in real-time.

Results: Twenty patients were enrolled for concurrent evaluation with both systems, which included 33 PGs and 19 non-parathyroid sites. NIRAF imaging demonstrated 90.9% sensitivity, 73.7% specificity, and 84.6% accuracy for PG identification when interpreted in real-time by the surgeon, as compared to 81.8% sensitivity, 73.7% specificity and 78.8% accuracy where images were quantitatively analyzed post hoc by an independent observer. In parallel, NIRAF detection with PTeye yielded 97.0% sensitivity, 84.2% specificity and 92.3% accuracy in real-time for the same specimens.

Conclusions: Both NIRAF-based systems were beneficial for identifying PGs intraoperatively. While NIRAF imaging provides valuable spatial information to localize PGs, NIRAF detection with fiber probe provides real-time quantitative information to identify PGs in presence of

ambient room lights.

Introduction

Inadvertent damage to or excision of a healthy parathyroid gland (PG) following a total thyroidectomy could result in transient hypocalcemia (< 6 months) in 5 – 35% of cases or permanent hypocalcemia (> 6 months) in up to 7% of the patients (1, 2). On the other hand, failed parathyroidectomies can occur in 5 – 10% of cases due to the inability to identify or localize the diseased PG (3, 4). As a result, persistent hyperparathyroidism can occur in these patients leading to unwarranted repeat surgeries that may be associated with increased morbidity and costs (5, 6). Ultrasound imaging, ^{99m}technetium-sestamibi scintigraphy, and computed tomography (CT) have demonstrated variable efficacy for preoperative localization of diseased PGs (7, 8). However, these modalities are unable to localize healthy PGs and may not always correlate well with the surgical field of view as observed intraoperatively. Consequently, most surgeons rely on visual identification of healthy or diseased PGs, whereby the accuracy of PG identification is eventually determined by her/his surgical skill and experience (9-11). When in doubt, a surgeon routinely confirms the identity of PG tissue by sending the specimen for frozen section analysis that typically requires a wait time of 20 – 30 minutes per sample (12) and has risk of possible injury to a healthy PG.

The unique discovery of near infrared autofluorescence (NIRAF) in PG tissues demonstrated that optical modalities that detect NIRAF can be exploited for non-invasive and label-free identification of both healthy and diseased PGs with an accuracy as high as 97% (13-16). As demonstrated by the Vanderbilt group, it was observed that PGs emit stronger NIRAF signal than the adjacent thyroid and other soft tissues in the neck. Since then, several research groups have explored the feasibility of localizing PGs using NIRAF detection with reasonable success (17-25). Based on the aforementioned studies that had been applied for PG localization,

optical modalities capable of NIRAF detection can be broadly categorized as (a) imaging systems and (b) fiber probe systems. Imaging systems, which are non-contact optical modalities, either tend to be commercially available near infrared (NIR) cameras (19, 21) or modified prototypes of existing imaging systems (15, 17, 22, 25). These imaging systems typically illuminate tissues with NIR light at a specific wavelength and collect the resultant fluorescence emitted from tissues with a hand-held camera. A fluorescent image is displayed on an adjacent display monitor and tissues with elevated NIRAF are seen as grey or pseudo-colored images for intraoperative visualization by the surgeon (**Figure 1**). In contrast, fiber probe systems involve placing a sterile hand-held fiber optic probe in contact with the tissue to capture tissue NIRAF as quantitative data. While this approach was highly sensitive in PG identification as evidenced from earlier studies, the data which are obtained in a 'spectral' format cannot be easily interpreted by surgeons (13, 14, 16). By improving on the original lab-built system, a newer iteration called PTeye (AiBiomed Inc., Santa Barbara, CA) was recently developed which provides the surgeon with real-time auditory feedback upon parathyroid identification along with a visual bar graph on the device display console (**Figure 2**). Compared to the lab-built system, PTeye has also demonstrated a high accuracy for PG identification with a relatively simpler user-interface and the ability to function even in the presence of ambient operating room (OR) lights, which tends to be a deterrent for most imaging systems (26, 27).

Since modalities that rely on NIRAF detection for label-free PG identification having been successfully validated in several studies (20, 26, 28, 29), FDA approval for this application was recently granted to Fluobeam, an imaging system, and PTeye, a fiber probe-based system, in 2018 (30, 31). Nonetheless, no study has directly compared the performance between these two approaches – imaging versus fiber probe – or assessed the value in PG identification by each

modality for the surgeon. The current prospective study was designed to compare the performance between an imaging and fiber probe-based approach in NIRAF detection by using the PDE-Neo II imaging system and the PTeye concurrently for the first time in a preliminary cohort of 20 patients. This study can help determine whether both systems are detecting similar NIRAF phenomena in PG tissues and potentially provide valuable insight into the benefits added by either modality in PG identification/localization inside the OR.

METHODS

Patient Recruitment.

Eligible patients who underwent thyroidectomy and/or parathyroidectomy between December 2018 and January 2019 at the Ohio State University Comprehensive Cancer Center were prospectively enrolled. This study was conducted in agreement with the Declaration of Helsinki and its amendments, and was approved by the Institutional Review Board (IRB) at Ohio State University (IRB# 201640045). Written informed consent was obtained from all enrolled patients prior to surgery. Acquired patient data were stored in compliance with the HIPAA privacy rule. Patients with a diagnosis of renal-induced secondary hyperparathyroidism were excluded from the study, as earlier studies had demonstrated irregularities in NIRAF observed among these patients (16, 26).

Routine preoperative, intraoperative and postoperative patient assessment.

Patients who underwent parathyroidectomy were preoperatively assessed with ultrasound and/or ^{99m}technetium-sestamibi nuclear imaging to aid in localizing diseased PGs, including parathyroid adenomas. Preoperative serum calcium levels, as well as preoperative, intraoperative, and immediate postoperative parathyroid hormone (PTH) levels were routinely measured for parathyroidectomy patients, while serum calcium levels were monitored

preoperatively and postoperatively for thyroidectomy patients. Excised specimens were subject to standard histopathologic analysis, including tissue type and disease, gross dimensions of the specimen, presence of parathyroid tissue in the specimen, normocellularity/hypercellularity and weight of excised parathyroid tissue.

Instrumentation of modalities relying on NIRAF detection

PDE-Neo II (Hamamatsu, Mitaka USA, Inc., Denver, CO) utilized for imaging in this study comprises: (i) a hand-held camera, (ii) a console for adjusting image acquisition parameters, and (iii) a display monitor mounted on a portable stand (**Figure 1**). The camera of PDE-Neo II emits NIR light at a wavelength of 760 nm using a light emitting diode (LED), with the device being categorized as a 1-M LED product. White light (true color) and NIRAF (grey/pseudo-colored green) images are relayed to the display monitor for visualization by the surgeon, as ambient OR lights are switched off during the procedure. In comparison, the fiber probe-based device, PTeye (**Figure 2**), comprises of (i) a console that consists of a 785 nm laser diode and a detector, (ii) a detachable fiber (optic) probe and (iii) a foot-pedal to activate NIRAF measurements. PTeye is also capable of detecting NIRAF without interference from ambient OR lights as well, due to the internal circuitry designed for the system. Tissue NIRAF recorded with PTeye is conveyed to a display panel of the console as well as to a loudspeaker for auditory feedback. The display panel informs the surgeon on (i) the 'Detection Level' – absolute tissue NIRAF intensity and (ii) the 'Detection Ratio' – tissue NIRAF normalized to the baseline NIRAF intensity which is translated into a percentage likelihood that the tissue is parathyroid up to 100%. The auditory feedback initiates when the 'Detection Ratio' exceeds 1.2 – the threshold value set for PG identification (26).

Comparative study with concurrent NIRAF detection with PDE-Neo II and PTeye.

During the surgery, tissue was identified as possible PG tissue by the surgeon and left *in situ*. Prior to NIRAF image acquisition, the handheld camera of PDE-Neo II was wrapped with a sterile transparent drape and positioned approximately 5 cm above the surgical field. After the OR lights were switched off, ambient white light (true color) images of the surgical field were first obtained with the camera followed by the corresponding NIRAF (pseudo-colored green) images (**Figure 1**) as described in an earlier study (32). If the PG was removed, the same procedure was performed for excised tissues *ex vivo* prior to these specimens being sent for routine histopathology. The surgeon's expert opinion on whether an *in situ* or excised tissue was PG or not, was first noted using only ambient white light visualization and then recorded again after the surgeon's real-time interpretation of the acquired NIRAF images. The surgeon's confidence in identifying PG(s) before and after imaging was semi-quantitatively denoted as the 'parathyroid identification confidence score,' measured on a scale of 1 (very low) to 5 (very high). If tissue sites were identified with low confidence score (2 or lower) and there was no corresponding histology available, NIRAF measurements for those sites were excluded from the study.

After image acquisition with PDE-Neo II, the surgeon repeated NIRAF assessments of the same tissue sites using PTeye with the OR lights remaining on. As the surgeon places the sterile fiber probe of PTeye on the tissue and presses the foot-pedal, tissue NIRAF intensity is then displayed in real-time on the device console display. During measurements with PTeye, it must be noted that the surgeon first establishes a NIRAF baseline for each patient by obtaining five successive NIRAF measurements on the patient's thyroid (or neck muscle, if thyroid was absent), following which subsequent measurements of 'Detection Level' and 'Detection Ratio' are recorded. Examples of a 'positive' and 'negative' measurement for PG as indicated on the

PTeye display are represented in **Figure 2B and 2C,** respectively. All PGs evaluated in this study were surgically exposed with adequate dissection prior to NIRAF detection with PDE-Neo II (imaging-based) or PTeye (fiber probe-based).

Data Analysis

For quantitative analysis, NIRAF images acquired with PDE-Neo II were retrospectively analyzed using the Image J software (National Institutes of Health, Bethesda, MD) by an independent, blinded and untrained observer. NIRAF intensity from at least 3 regions of equal dimensions within areas of maximum fluorescence (brightest region) in the image was averaged and normalized to the background noise in order to generate NIRAF-to-background ratio (NBR) for each image. For *in situ* images of potential PGs, background noise was quantified from areas of adjacent soft tissues e.g. thyroid. In contrast, when excised tissues were imaged, the background noise was measured from areas of the 'non-tissue background' due to lack of adjacent soft tissues in the image. Continuous variables such as NBRs for PDE-Neo II and Detection Ratios (as described earlier) for PTeye were then averaged accordingly for concurrently assessed PG tissues and non-PG tissues and reported as mean $\pm$ standard error with the inter-quartile range (IQR). Differences in these measured ratios were analyzed using the 2-tailed *t*-test for unequal variance. A paired *t*-test was utilized for assessing the change in parathyroid identification confidence score from the surgeon before and after NIRAF imaging. For these analyses, a p-value lower than 0.05 was considered statistically significant. Detection rate for each system was determined by correlating the number of tissues deemed PG positive by the system (Threshold: NBR > 1.10 for PDE-Neo II (32); Detection Ratio > 1.2 for PTeye (26, 27)) with the number of PG tissues confirmed using histology for excised or biopsied PGs, or visual inspection by participant surgeons for *in situ* PGs (assessed with a parathyroid

identification confidence score > 2).

RESULTS

Patient Demographics

Twenty patients assessed concurrently with both NIRAF detection-based systems were enrolled for this study, which consisted of 16 women (80%) and 4 men (20%). Clinicopathologic features are summarized in **eTable 1**. The median age was 59 years [IQR: 41.5–64.5 years], while the median body mass index was 27.8 kg/m^2 [IQR: 24.5–34.1 kg/m^2]. Surgical procedures included 6 total thyroidectomies (with or without central neck dissection), 3 thyroid lobectomies, 1 completion thyroidectomy, 1 completion central neck dissection (with previous total thyroidectomy), 1 combined total thyroidectomy-parathyroidectomy and 8 parathyroidectomies. All 9 patients who underwent parathyroidectomy had preoperative ultrasound performed, while 4 patients underwent preoperative ^{99m}technetium-sestamibi nuclear imaging. Ultrasound was able to preoperatively visualize diseased PG(s) in 8 out of 9 patients (88.9%), while ^{99m}technetium-sestamibi imaging could localize hyper-functioning PG(s) in 3 out of 4 patients (75.0%). A total of 12 PGs were excised for histological analysis, among which 2 glands were normocellular while 10 glands were hypercellular. Among the two excised normocellular PGs, one gland was found in conjunction with thymic tissue making it appear larger than its true size and was presumed as 'diseased' by the surgeon, while the other gland was found associated with adjacent medullary thyroid cancer in a thyroidectomy patient.

Device Performance of NIRAF-based modalities

Concurrent assessment with PDE-Neo II and PTeye was performed on 33 PGs (23 healthy and 10 diseased PGs) and 19 non-parathyroid sites (thyroid, mediastinal soft tissues, lymph nodes, yellow and brown fat) either *in situ* or *ex vivo* for the enrolled patients. Surgical

field of view as displayed on the device monitor when visualized using PDE-Neo II with ambient white light has been depicted in **Figure 3 (A, C, E, G, I)** and subsequently with corresponding NIR illumination in **Figure 3 (B, D, F, H, J)**. PG tissues were observed to have stronger NIRAF intensity than that of the non-parathyroid sites when subjectively interpreted in real-time by the surgeon in the OR, as well as when the acquired NIRAF images were retrospectively and quantitatively analyzed by an independent untrained observer. Quantitative analysis revealed that the mean NBR of PGs (n = 33) measured 1.24 ± 0.03 (IQR: 1.12 – 1.31), while the mean NBR of non-parathyroid sites (n = 19) measured significantly lower at 1.12 ± 0.04 (IQR: 1.00 – 1.16; p-value = 0.013). Mean NBR from diseased PGs measured significantly higher than that of healthy PGs (1.38 ± 0.07 vs. 1.17 ± 0.02; p-value = 0.02). Mean NBR for all PGs imaged also measured higher *ex vivo* than NBR *in situ* (1.41 ± 0.08 vs. 1.17 ± 0.02; p-value = 0.010).

Unlike PDE-Neo II, quantitative parameters, such as 'Detection Ratio', were output in real-time with PTeye, as displayed in **Figure 2**. In agreement with results of imaging approach, the mean Detection Ratio with PTeye was also considerably higher for PGs at 3.55 ± 0.27 (IQR: 2.06 – 4.07) compared to non-parathyroid tissues that measured 1.33 ± 0.52 (IQR: 0.38 – 0.95; p-value = 0.0007). However, in contrast with PDE-Neo II, no significant difference was observed between Detection Ratios of diseased and healthy PGs at 4.06 ± 0.53 and 3.26 ± 0.29 respectively (p-value = 0.20). Similarly, no notable difference in Detection Ratios was observed between *ex vivo* and *in situ* measurements for PG specimens: 3.97 ± 0.60 vs. 3.34 ± 0.27 (p-value = 0.35). A comparative overview of quantitative parameters such as NBRs and Detection Ratio between both the systems is provided in **Table 1**.

In terms of device performance for PG identification, PDE-Neo II provided 90.9% sensitivity, 73.7% specificity and 84.6% overall accuracy (**Table 2**) when based on the surgeon's

real-time interpretation of NIRAF images. The sensitivity of imaging in detecting NIRAF from PGs was further reflected with a significant increase in the surgeon's mean parathyroid identification confidence score. Upon using just ambient white light, the surgeon's confidence score stood at 3.91 ± 0.09, while significantly improving to 4.17 ± 0.02 after imaging (+0.26, p-value = 0.006). With retrospective quantification of the same NIRAF images analyzed post hoc by an independent observer, PDE-Neo II demonstrated 81.8% sensitivity, 73.7% specificity, and 78.8% overall accuracy in PG identification. In comparison to imaging, NIRAF detection with PTeye yielded 97.0% sensitivity, 84.2% specificity and 92.3% overall accuracy in PG identification on the basis of real-time output of Detection Ratios. Of the 12 PG specimens (10 diseased and 2 healthy) that were resected and validated with histology, PG detection rate was 91.7% for PDE-Neo II (11/12 PGs) based on surgeon's real-time interpretation and 75.0% (9/12 PGs) with post hoc analysis of NIRAF images, versus 100% for PTeye (12/12 PGs based on device output). More importantly, real-time interpretation with PDE-Neo II as well as PTeye aided in intraoperative identification of diseased PGs that were not preoperatively localized in 11.1% of patients who had an ultrasound (1/9 patients) and 25.0% of patients who underwent ^{99m}technetium-sestamibi scans (1/4 patients).

DISCUSSION

The discovery of NIRAF of PGs at Vanderbilt University has led to a surge of studies that exploited this unique property of PG tissues using modalities capable of NIRAF detection. The popularity of this method is a result of its label-free nature, thereby overcoming the limitations of intraoperative imaging typically associated with methylene blue, indocyanine green (ICG), or intraoperative scintigraphy, all of which require contrast agent injection (33-35). As the etiology behind NIRAF in PG tissues is still being investigated (36, 37), the majority of studies have

relied on detection of NIRAF for intraoperative PG identification via imaging systems, while only studies from the Vanderbilt group have utilized the fiber probe-based approach of NIRAF detection for the same application. The lone study that included both imaging and fiber probe-based methods of NIRAF detection did not compare the two approaches concurrently, while using a non-commercially available NIRAF imaging system (modified from a Karl Storz camera) in 9 patients (27). The current study is the first one to report on the direct comparison between the imaging (non-contact based) and fiber probe (contact-based) approaches in NIRAF detection, which was performed concurrently in a single cohort of patients for intraoperative PG identification. PDE-Neo II (Hamamatsu) and PTeye served as the representative devices for imaging and fiber probe-based systems respectively, where both these modalities are commercially available and rely on NIRAF detection from PG tissues.

Based on our results, NIRAF of PG tissues were considerably higher than other soft tissues of the neck, including the thyroid gland, when tested with either NIRAF detection-based modalities, in agreement with earlier study observations (16, 17, 19, 21, 26, 32). Upon assessing the device performance in this small cohort of patients, NIRAF detection with the fiber probe-based device demonstrated a higher accuracy of 92.3% in PG identification as compared to 78.8 – 84.6% yielded by the imaging-based approach (**Table 2**). Better sensitivity in identifying PGs with PTeye (97.0%) could be due to the fact that the fiber probe is in direct contact with the tissue whereas the camera of the PDE-Neo II is typically held at a distance of 5 cm from the surgical field, akin to other imaging system cameras (38). However, since the fiber probe of PTeye requires tissue contact (**Figure 2D, 2E**), the modality requires the probe to be sterile prior to use in each patient. On the other hand, while imaging systems does not require tissue contact, the camera still requires a transparent sterile barrier drape (**Figure 1B**), as contemporary NIR

cameras cannot capture sensitive images beyond a distance of 45 cm (18 inches) from the surgical field, which is the recommended 'sterile zone' in an OR (39).

While comparing the performance between imaging and fiber probe-based approaches in NIRAF detection, it is also worth noting that different excitation wavelengths were used by each modality – 760 nm for PDE-Neo II and 785 nm for PTeye. While the difference in excitation wavelengths is ostensibly small, this difference may influence intensity of NIRAF emitted by PG tissues. Illuminating the target fluorophore (in tissue) at an excitation wavelength more closely matched to its peak absorption wavelength could result in fluorescence at a greater intensity. It is currently not clear to what extent the differences in excitation wavelength between PDE-Neo II and PTeye may have impacted the performance of these two devices in detecting NIRAF emitted from the assessed PG tissues. Nonetheless, determining the optimal excitation wavelength for PG localization/identification needs to be considered and explored further in later iterations of these devices.

A somewhat surprising finding in our study was that the accuracy of imaging in PG identification was higher when NIRAF images were interpreted in real-time by an expert surgeon (>10 years of experience) as compared to when the same images were quantitatively analyzed post hoc by an independent blinded and untrained observer. Several factors may have contributed to this unexpected finding. Primarily, the surgeon is able to move the camera during the procedure to image an area of interest from slightly different angles, which provides a better three-dimensional view rather than a single two-dimensional image as analyzed retrospectively by the independent observer. Secondly, NIRAF images as viewed by surgeon on the monitor (for which the imaging system is optimized) may be of a better quality than the saved images that were retrospectively analyzed. Finally, NIRAF image assessment (Figure **1C, 3F**) can be

subjective and may be misinterpreted without sufficient surgical training or experience. Therefore, PG identification with intraoperative NIRAF imaging may also partially depend on the surgeon's expertise compared to an independent untrained evaluator. While the imaging-based approach lacks real-time quantitative information or an identification threshold for confirming PGs, this limitation has been offset in the fiber probe-based modality, where PTeye provides a NIRAF-related 'Detection Level' and 'Detection Ratio' instantly for the end-user. Nonetheless, the comparative benefit from an imaging versus fiber probe-based approach for intraoperative PG identification needs to eventually be validated in larger cohorts and for surgeons with nominal experience.

Differences in how tissue NIRAF is normalized for PDE-Neo II (imaging) and PTeye (fiber probe) could also affect data interpretation for each system. For post hoc quantitative analysis with imaging systems, tissue NIRAF is typically normalized to background autofluorescence to generate NIRAF-to-background ratio (NBR). This mode of normalization may have its limitations, as background autofluorescence can fluctuate significantly across different anatomical sites as well as between *in situ* and *ex vivo* locations. It should be reiterated here that *in situ* background autofluorescence from thyroid and other soft-tissues in the neck would be higher when compared to that in an *ex vivo* setting. Therefore, it would be understandable as to why PGs imaged *in situ* yielded considerably lower NBRs than those imaged *ex vivo* as observed in our study, which was also in agreement with the findings of Squires *et al.* (32) It might also explain as to why NBRs quantified from diseased PGs were considerably higher than that from healthy PGs, as majority of the diseased glands (7/10 PGs) were imaged *ex vivo* in this study, in contrast to healthy PGs that were always visualized *in situ*. This trend was however not observed with PTeye, since tissue NIRAF was normalized instead to

a steady parameter – the baseline thyroid NIRAF, which does not fluctuate, unlike background autofluorescence that varies across different imaging fields. Consequently, there was no significant difference observed with PTeye in the Detection Ratio between (i) diseased and healthy PGs or (ii) *in situ* and *ex vivo* PGs. Furthermore, it should be duly considered that tissue NIRAF normalization to a steady baseline parameter, such as thyroid NIRAF would be reliable only if NIRAF intensities of the 'target tissue' and 'background thyroid' were measured from the same distance by the device detectors, namely the fiber probe for PTeye or handheld camera for PDE-Neo II. Since PTeye is a contact-based approach, the distance between the fiber probe and the target tissue/thyroid is always zero and thus stays constant, due to which tissue NIRAF can be reliably normalized to thyroid NIRAF, which then serves as a steady baseline parameter. In contrast, this mode of normalization may not be applicable for imaging with PDE-Neo II, as it becomes challenging for a surgeon to ensure that the device camera is consistently held at the exact same distance for tissues being imaged at all times in an OR setting. Since NIRAF intensity can fluctuate significantly between images due to variable distance between the handheld camera and tissues, it may not be accurate to normalize tissue NIRAF from a 'target tissue' to that of the thyroid gland, either of which may have been imaged at different distances from the camera. Therefore, it would be more practical to normalize tissue NIRAF to the background fluorescence measured in the same image than to thyroid NIRAF from another image, when using an imaging-based approach as with PDE-Neo II.

Both approaches of NIRAF detection – based on imaging and fiber probe – are equipped with a distinct set of salient features as provided in **Table 3**. Due to lack of spatial information provided with PTeye, the surgeon needs to first visualize the 'suspect PG' tissue beforehand prior to confirmation with the device. In comparison, imaging systems such as PDE-Neo II and

other equivalent instruments are capable of wide-field imaging for NIRAF detection, which can be extremely valuable for spatially localizing PGs during head and neck surgeries. As a result, certain studies have explored the feasibility for 'mapping' PGs during operative surgeries with reasonable success, even being able to visualize NIRAF of PGs below layers of fibrofatty tissue by using a custom-built imaging system (22, 24, 25, 40). However, the ability to localize 'missing' or 'hidden' PGs using NIRAF detection has not been reported with consistent success across different groups. For instance, DiMarco *et al.* found that the commercial imaging system employed for NIRAF detection in their study failed to find the 'missing' PGs that could not be localized by the operating surgeon (37). Similar findings were also observed with our current study where PGs in Patient 6 could not be visualized either by the surgeon or both NIRAF detection-based modalities. Disparities in the various studies, including our current findings, may be due to differences in the NIRAF detection threshold of the cameras utilized across these studies. Since NIR wavelengths can typically penetrate only a few millimeters of tissue, the ability to localize missing PGs will highly depend on the camera sensitivity, the NIR irradiance employed, and optical properties of the tissues that overlie the hidden PGs. Therefore, while commercially available imaging systems might be limited currently in being able to localize missing or hidden PGs, the preliminary results of Kim *et al.* are promising and indicate that specific iterations to imaging systems may eventually ensure NIRAF-based spatial mapping even for hidden PGs (22, 24, 40).

Since imaging with PDE-Neo II does not involve tissue contact, NIRAF detection of PG becomes problematic with increasing distance between the camera and the location of PG. As a result, localization of deep-seated PGs or ectopic PGs may require more extensive surgical dissection or wider incisions in the neck to obtain optimal NIRAF images with the camera. These

issues with imaging can be further compounded when other strong sources of NIRAF – surgical kittner, surgical drape, adjacent parathyroid – are present in the surgical field of view, as it can obscure NIRAF of the main target PG. These limitations are minimized with PTeye, as the hand-held fiber probe can be conveniently positioned onto the target site, irrespective of PG location or extraneous sources of NIRAF in the surgical field.

With regard to incorporating NIRAF detection approaches during surgical procedures, it must be noted that OR lights must be off prior to use of most imaging systems, as these tend to interfere with NIRAF detection in the surgical field, potentially disrupting conventional surgical work-flow (15, 27). On the contrary, the system design of PTeye ensures that the device can measure tissue NIRAF even in the presence of OR lights, making it a relatively easier modality to implement in a manner similar to other contact-based modalities, such as nerve monitoring devices, already being used in head and neck operations (41). Considering device compatibility with OR lights, a newer generation imaging system called Fluobeam LX was recently showcased, where the device is described as being able to detect tissue NIRAF without interference from OR lights (42). In terms of device utility for intraoperative surgical guidance, the performance of PTeye has been validated only for label-free parathyroid identification till date (26, 27), and its scope for other applications remains to be explored. On the other hand, imaging systems such as PDE-Neo II have successfully demonstrated feasibility for various applications besides parathyroid localization, such as tissue angiography, tumor margin demarcation, and lymph node mapping (38).

Although promising results were obtained with both imaging and fiber probe-based approaches for NIRAF detection in our study, these modalities should currently serve as adjuncts for label-free intraoperative PG identification. Surgical skill and expertise should still remain

pivotal for localizing, identifying and eventually preserving PGs. At present, modalities capable of detecting NIRAF for intraoperative PG identification would probably be more beneficial for (i) surgeons with nominal experience or training in head and neck operations (9, 10, 43), (ii) patients with multi-gland parathyroid disease or aberrant-ectopic PGs (11), (iii) re-operative surgeries with distorted anatomy (44), and (iv) surgeries for malignant thyroid disease (45). A prime advantage gained in these scenarios would involve identifying PGs missed by preoperative localization with ultrasound or ^{99m}technetium-sestamibi scans – as demonstrated with our results – thereby minimizing frozen biopsies sent for PG confirmation leading to potential reduction in OR procedure time and associated costs. Certain studies have investigated the impact of NIRAF detection-based imaging on patient outcomes in thyroid and parathyroid surgeries by using different commercial systems such as Fluobeam and PDE-Neo II with variable results (20, 32, 37, 46), while outcome studies using fiber probe-based approaches i.e. PTeye are currently underway. However, there is a further need to conduct larger, long-term outcome studies that would evaluate the cost-benefit ratio associated with the use of modalities that can detect NIRAF to minimize postsurgical morbidity and unnecessary expenses.

Conclusions

Two different optical modalities based on NIRAF detection were found to potentially serve as valuable tools for sensitively identifying healthy and diseased PGs intraoperatively, and could be of substantial benefit in ensuring optimal patient outcomes following thyroid and parathyroid surgeries. Imaging based on NIRAF detection can guide PGs localization in relation to adjacent anatomic structures by providing valuable spatial information. In parallel, fiber probe-based NIRAF detection can successfully provide real-time quantitative information that can aid in objectively confirming PG tissue in real-time, even in presence of ambient OR lights.

Acknowledgments

We would like to thank the OR staff for their assistance in data collection.

References

1. Antakia R, Edafe O, Uttley L, Balasubramanian SP. Effectiveness of Preventative and Other Surgical Measures on Hypocalcemia Following Bilateral Thyroid Surgery: A Systematic Review and Meta-Analysis. Thyroid. 2014;25:95-106.

2. Edafe O, Antakia R, Laskar N, et al. Systematic review and meta-analysis of predictors of post-thyroidectomy hypocalcaemia. The British journal of surgery. 2014 Mar;101(4):307-20.

3. Simental A, Ferris RL. Reoperative Parathyroidectomy. Otolaryngologic Clinics of North America. 2008 2008/12/01/;41(6):1269-74.

4. Cron DC, Kapeles SR, Andraska EA, et al. Predictors of operative failure in parathyroidectomy for primary hyperparathyroidism. The American Journal of Surgery. 2017;214:509-14.

5. Doherty GM, Weber B, Norton JA. Cost of unsuccessful surgery for primary hyperparathyroidism. Surgery. 1994;116(6):954-8.

6. Wachtel H, Cerullo I, Bartlett EK, et al. What Can We Learn from Intraoperative Parathyroid Hormone Levels that Do Not Drop Appropriately? Annals of Surgical Oncology. 2015 June 01;22(6):1781-8.

7. Mohebati A, Shaha AR. Imaging techniques in parathyroid surgery for primary hyperparathyroidism. American Journal of Otolaryngology. 2012 12/07;33(4):457-68.

8. Ahuja AT, Wong KT, Ching ASC, et al. Imaging for primary hyperparathyroidism — what beginners should know. Clinical Radiology. 2004 11//;59(11):967-76.

9.   Sosa JA, Bowman HM, Tielsch JM, et al. The Importance of Surgeon Experience for Clinical and Economic Outcomes From Thyroidectomy. Annals of Surgery. 1998;228(3):320-30.

10.   Sosa JA, Powe NR, Levine MA, et al. Thresholds for Surgery and Surgical Outcomes for Patients with Primary Hyperparathyroidism: A National Survey of Endocrine Surgeons. The Journal of Clinical Endocrinology & Metabolism. 1998;83(8):2658-65.

11.   Chen H, Wang TS, Yen TWF, et al. Operative Failures After Parathyroidectomy for Hyperparathyroidism: The Influence of Surgical Volume. Annals of Surgery. 2010;252(4):691-5.

12.   Novis DA, Zarbo RJ. Interinstitutional comparison of frozen section turnaround time. Archives of pathology & laboratory medicine. 1997;121(6):559.

13.   Paras C, Keller M, White L, et al. Near-infrared autofluorescence for the detection of parathyroid glands. Journal of Biomedical Optics. 2011;16(6):067012--4.

14.   McWade MA, Paras C, White LM, et al. A novel optical approach to intraoperative detection of parathyroid glands. Surgery. 2013 12//;154(6):1371-7.

15.   McWade MA, Paras C, White LM, et al. Label-free Intraoperative Parathyroid Localization With Near-Infrared Autofluorescence Imaging. The Journal of Clinical Endocrinology & Metabolism. 2014;99(12):4574-80.

16.   McWade MA, Sanders ME, Broome JT, et al. Establishing the clinical utility of autofluorescence spectroscopy for parathyroid detection. Surgery. 2016 1//;159(1):193-203.

17.   Ladurner R, Sommerey S, Arabi NA, et al. Intraoperative near-infrared autofluorescence imaging of parathyroid glands. Surgical Endoscopy. 2016:1-6.

18.   Ladurner R, Al Arabi N, Guendogar U, Hallfeldt KKJ, Stepp H, Gallwas JKS. Near-infrared autofluorescence imaging to detect parathyroid glands in thyroid surgery. Annals of the Royal College of Surgeons of England. 2018;100:33-6.

19.   Falco J, Dip F, Quadri P, et al. Increased identification of parathyroid glands using near infrared light during thyroid and parathyroid surgery. Surgical Endoscopy. 2017 September 01;31(9):3737-42.

20.   Dip F, Falco J, Verna S, et al. Randomized Controlled Trial Comparing White Light with Near-Infrared Autofluorescence for Parathyroid Gland Identification During Total Thyroidectomy. Journal of the American College of Surgeons. 2019;228:744-51.

21.   Shinden Y, Nakajo A, Arima H, et al. Intraoperative Identification of the Parathyroid Gland with a Fluorescence Detection System. World Journal of Surgery. 2017 June 01;41(6):1506-12.

22.   Kim SW, Song SH, Lee HS, et al. Intraoperative real-time localization of normal parathyroid glands with autofluorescence imaging. The Journal of Clinical Endocrinology & Metabolism. 2016;101(12):4646-52.

23.   Kim SW, Lee HS, Ahn Y-C, et al. Near-Infrared Autofluorescence Image-Guided Parathyroid Gland Mapping in Thyroidectomy. Journal of the American College of Surgeons. 2018;226(2):165-72.

24.   Kim SW, Lee HS, Lee KD. Intraoperative real-time localization of parathyroid gland with near infrared fluorescence imaging. Gland surgery. 2017;6(5):516.

25.   Kim Y, Kim SW, Lee KD, Ahn Y-c. Real-time localization of the parathyroid gland in surgical field using Raspberry Pi during thyroidectomy: a preliminary report. Biomedical optics express. 2018;9(7):3391-8.

26. Thomas G, McWade MA, Paras C, et al. Developing a clinical prototype to guide surgeons for intraoperative label-free identification of parathyroid glands in real time. Thyroid. 2018;28(11):1517-31.

27. Thomas G, McWade MA, Nguyen JQ, et al. Innovative surgical guidance for label-free real-time parathyroid identification. Surgery. 2019;165(1):114-23.

28. Kahramangil B, Dip F, Benmiloud F, et al. Detection of Parathyroid Autofluorescence Using Near-Infrared Imaging: A Multicenter Analysis of Concordance Between Different Surgeons. Annals of Surgical Oncology. 2018;25:957-62.

29. Benmiloud F, Rebaudet S, Varoquaux A, et al. Impact of autofluorescence-based identification of parathyroids during total thyroidectomy on postoperative hypocalcemia: a before and after controlled study. Surgery. 2017 2017/11/06/.

30. The United States Food and Drug Administration. FDA permits marketing of two devices that detect parathyroid tissue in real-time during surgery. Available at: https://www.fda.gov/NewsEvents/Newsroom/PressAnnouncements/ucm624982.htm. Accessed November 3, 2018.

31. Voelker R. Devices Help Surgeons See Parathyroid Tissue. Jama. 2018;320:2193.

32. Squires MH, Jarvis R, Shirley LA, Phay JE. Intraoperative Parathyroid Autofluorescence Detection in Patients with Primary Hyperparathyroidism. Annals of Surgical Oncology. 2019;26:1142-8.

33. Han N, Bumpous JM, Goldstein RE, et al. Intra-operative parathyroid identification using methylene blue in parathyroid surgery. The American surgeon. 2007;73(8):820-3.

34.   Zaidi N, Bucak E, Yazici P, et al. The feasibility of indocyanine green fluorescence imaging for identifying and assessing the perfusion of parathyroid glands during total thyroidectomy. Journal of Surgical Oncology. 2016;113(7):775-8.

35.   Koc ZP, Ozcan Kara P, Dag A, Berkesoglu M. Feasibility of portable gamma camera imaging in intraoperative radioguided parathyroid adenoma identification. Iranian Journal of Nuclear Medicine. 2018;26:62-5.

36.   Thomas G, McWade MA, Sanders ME, et al. Identifying the novel endogenous near-infrared fluorophore within parathyroid and other endocrine tissues. Optical Tomography and Spectroscopy; 2016: Optical Society of America; 2016. p. PTu3A. 5.

37.   DiMarco A, Chotalia R, Bloxham R, et al. Autofluorescence in Parathyroidectomy: Signal Intensity Correlates with Serum Calcium and Parathyroid Hormone but Routine Clinical Use is Not Justified. World Journal of Surgery. 2019;43:1532-7.

38.   Zhu B, Sevick-Muraca E. A review of performance of near-infrared fluorescence imaging devices used in clinical studies. The British journal of radiology. 2014;88(1045):20140547.

39.   Price P, Frey KB. Microbiology for surgical technologists: Cengage Learning; 2003.

40.   Kim SW, Lee HS, Ahn Y-C, et al. Near-Infrared Autofluorescence Image-Guided Parathyroid Gland Mapping in Thyroidectomy. Journal of the American College of Surgeons. 2018;226:165-72.

41.   Angelos P. Recurrent laryngeal nerve monitoring: state of the art, ethical and legal issues. Surgical Clinics. 2009;89(5):1157-69.

42. Fluobeam® LX: A breakthrough innovation for thyroid and parathyroid surgery. Available at: https://fluoptics.com/en/fluobeam-lx-breakthrough-innovation-thyroid-surgery/. March 29, 2019.

43. Adam MA, Thomas S, Youngwirth L, et al. Is There a Minimum Number of Thyroidectomies a Surgeon Should Perform to Optimize Patient Outcomes? Annals of Surgery. 2017;265(2):402-7.

44. Lin DT, Patel SG, Shaha AR, et al. Incidence of Inadvertent Parathyroid Removal During Thyroidectomy. The Laryngoscope. 2002;112(4):608-11.

45. Bergamaschi R, Becouarn G, Ronceray J, Arnaud JP. Morbidity of thyroid surgery. The American Journal of Surgery. 1998 1998/07/01/;176(1):71-5.

46. Benmiloud F, Rebaudet S, Varoquaux A, et al. Impact of autofluorescence-based identification of parathyroids during total thyroidectomy on postoperative hypocalcemia: a before and after controlled study. Surgery. 2018;163(1):23-30.

Table 1: Overview of Near Infrared Autofluorescence (NIRAF)-Related Quantitative Parameters

Measured Concurrently with Imaging and Fiber Probe-Based Approaches

Parameter	n	Mean ± SD	p Value
NBR with PDE-Neo II (imaging-based)			
Total PG	33	1.24 ± 0.03	0.013*
Total non-parathyroid tissue	19	1.12 ± 0.04	
Healthy PG	23	1.17 ± 0.02	0.02*
Diseased PG	10	1.38 ± 0.07	
In situ PG	21	1.17 ± 0.02	0.01*
Excised PG	12	1.41 ± 0.08	
Detection ratios with PTeye (fiber probe-based)			
Total PG	33	3.55 ± 0.27	0.0007*
Total non-parathyroid tissue	19	1.33 ± 0.52	
Healthy PG	23	3.26 ± 0.29	0.20
Diseased PG	10	4.06 ± 0.53	
In situ PG	21	3.34 ± 0.27	0.35
Excised PG	12	3.97 ± 0.60	

*p value < 0.05 (statistically significant based on 2-tailed *t*-test for unequal variance)
NBR, near infrared autofluorescence (NIRAF)-to-background ratio**,** PG, parathyroid gland

Table 2: Comparison of Parathyroid Gland Identification Rates and Device Performance

between PDE-Neo II (Imaging-Based) and PTeye (Fiber Probe-Based) across 20 patients

Variable	Imaging – PDE-Neo II camera (real-time image interpretation by expert surgeon)	Imaging – PDE-Neo II camera (post hoc image analysis by independent observer)	Fiber probe – PTeye (real-time data output)
Performance	NIRAF detection with imaging	NIRAF detection with imaging	NIRAF detection with fiber probe
PG assessed (P=33), p/P (%)			
Identification rate	30/33 (90.9)	27/33 (81.8)	32/33 (97.0)
Healthy	20/23 (87.0)	19/23 (82.6)	22/23 (95.7)
Diseased	10/10 (100.0)	8/10 (80.0)	10/10 (100.0)
Sensitivity	30/33 (90.9)	27/33 (81.8)	32/33 (97.0)
Non-PG site assessed (NP=19)			
Specificity, np/NP (%)	14/19 (73.7)	14/19 (73.7)	16/19 (84.2)
Positive predictive value, %	85.7	84.4	91.4
Negative predictive value, %	82.4	70.0	94.1
False negative rate, %	9.1	18.2	3.0
False positive rate, %	26.3	26.3	15.8
Overall accuracy, κ value (%)	κ = 0.66 (84.6)	κ = 0.55 (78.8)	κ = 0.83 (92.3)

Non-PG sites assessed: thyroid lobes, lymph node, central neck or lateral neck or mediastinal tissues, yellow & brown fat.

NIRAF, near infrared autofluorescence; np, device negative for parathyroid; NP, true negative – non-parathyroid tissue; p, device positive for parathyroid; P, true positive – parathyroid tissue; PG, parathyroid gland

Table 3: Overview of the Salient Features, Merits, and Demerits of Imaging vs Fiber Probe-based Approaches in Near Infrared Autofluorescence (NIRAF) Detection for Intraoperative Parathyroid Identification

Feature	Imaging-based approach of NIRAF detection	Fiber probe-based approach of NIRAF detection
Model	PDE-Neo II (Hamamatsu)	PTeye (AiBiomed)
Data output	NIRAF images (grey or pseudo-colored green) and white light images (true color) on display monitor	NIRAF detection intensity, NIRAF detection ratio
Dimension	Camera unit: 8 cm × 18.2 cm × 8 cm Console: 32.2 cm × 28.3 cm × 5.5 cm (excluding display monitor and stand).	Probe: Rigid tip portion (hand-held) - 16 cm long. Flexible portion (connected to console) - 234 cm long Console: 33 cm × 21.6 cm × 14 cm
Functional component	Portable near infrared camera	Hand-held fiber-optic probe for point-based NIRAF detection
Laser source	760 nm light emitting diode	785 nm laser diode
Spatial information	Yes	None
Working distance from surgical field	5 cm (near focus) to 30 cm (far focus)	Contact-based modality
Surgical field of view per measurement	10 cm × 10 cm	600 μm wide (point-based measurement)
Auditory feedback	No	Yes
Visual feedback	Remote display monitor	Console display interface
Contrast agents	Not required	Not required
Ambient OR light interference	Yes	No
Commercial availability	Yes	Yes
FDA approval for label-free intraoperative PG identification	Not at present for PDE-Neo II. (Approval granted for 'Fluobeam' – another NIRAF imaging system)	Yes
Advantage	Wide-field imaging technique	A more compact unit
	Spatial information of parathyroid acquired	Hand-held point-based guidance technique
	Multi-functional device; can be used for other surgical guidance	Provides real-time quantitative information

	applications in conjunction with contrast agents: lymph node surveillance, tumor margin demarcation, perfusion assessment of PG or other tissues	
	-	Functional with ambient OR lights
Disadvantage	Affected by ambient OR lights	No spatial information provided
	NIRAF signal affected by varying distance of camera from surgical field	Sterility of probe is required as the modality is contact-based
	No real-time quantitative information provided	Cannot localize hidden or missing PG; prospective PG needs to be visualized before assessment with device
	NIRAF image interpretation is subjective and would depend on surgeon experience	Error in baseline NIRAF acquisition could provide inaccurate results
	Wider neck incision required for NIRAF image acquisition	-
	Weaker NIRAF signal from deeper PG	-

NIRAF, near infrared autofluorescence; OR, operating room; PG, parathyroid gland

Figure Legends

Figure 1: (A) A clinical imaging system – PDE-Neo II – tested for intraoperative parathyroid gland (PG) identification, based on near infrared autofluorescence (NIRAF) detection. (B) The hand-held camera of the system is sterile wrapped with a transparent drape prior to NIRAF imaging. (C) Tissue NIRAF visualized on the remote display monitor of the system in pseudo-colored green. PG tissue (within yellow dashed circle) is observed to have a stronger NIRAF compared to adjacent soft tissue.

Figure 2: (A) A clinical fiber probe-based system – PTeye – utilized for intraoperative parathyroid gland (PG) identification, based on near infrared autofluorescence (NIRAF) detection. PTeye consists of 1) the console that has a display and encloses the near infrared laser and the detector, 2) a detachable fiber optic probe, and 3) a foot-pedal which is activated by the surgeon for tissue NIRAF measurements. (B & C) The display monitor on PTeye indicates if the tissue in contact with the probe is parathyroid (left) or not (right). (D & E) The fiber-optic probe can be utilized for confirming if the tissue is parathyroid whether it is in situ (left) or ex vivo (right) with ambient operation room lights remaining on.

Figure 3: White light (left) and NIRAF image in pseudo-colored green (right) taken with PDE-Neo II for (A, B) a healthy PG in situ, (C, D) in situ thyroid lobe, (E, F) a diseased PG in situ, (G, H) a diseased PG ex vivo and (I, J) a diseased PG and a lymph node ex vivo. Note that PG tissues exhibit stronger NIRAF compared to the non-parathyroid tissues (thyroid, lymph node) or the background. (NIRAF – Near infrared autofluorescence, PG – parathyroid gland, LN – lymph node)

Precis

Near infrared autofluorescence (NIRAF) can guide intraoperative parathyroid gland identification. Devices that can detect NIRAF typically rely on imaging or fiber probe-based approaches. This prospective study compared both these approaches for the first time, when tested concurrently in a preliminary cohort of 20 patients.
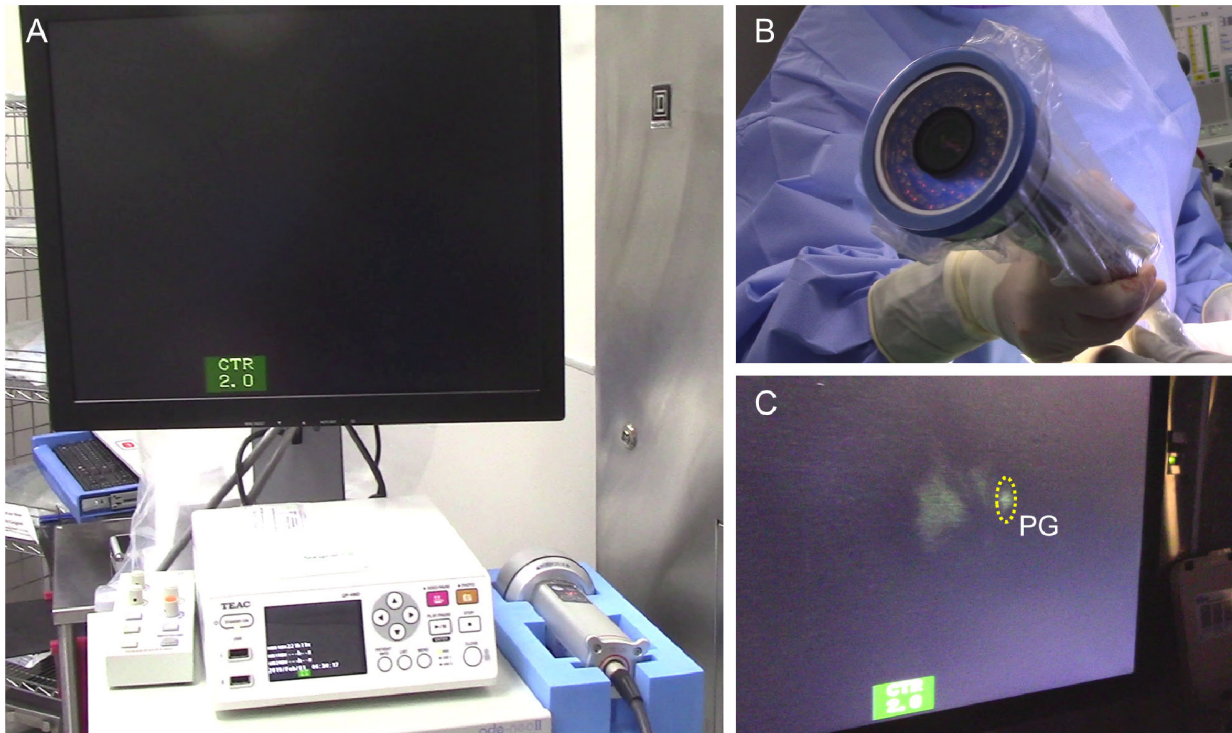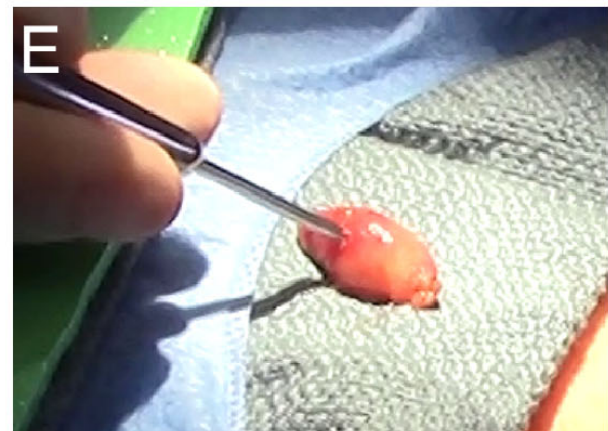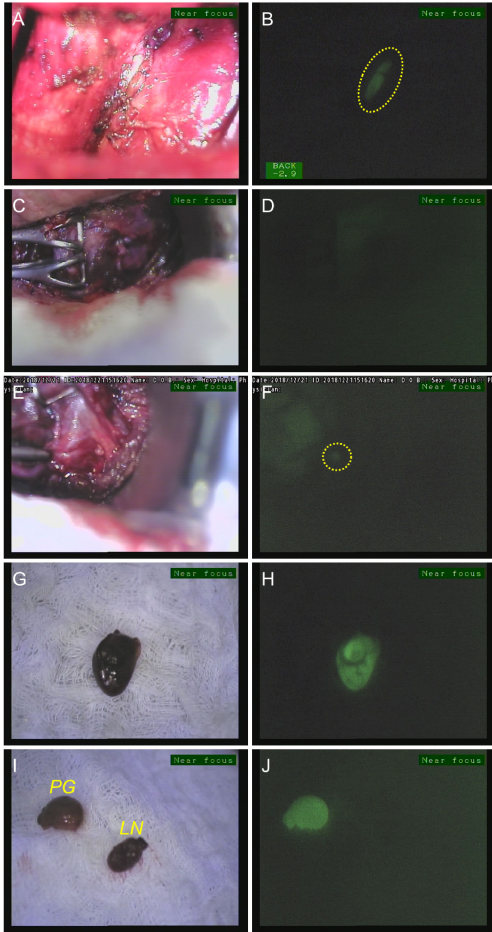
eTable 1: Demographics and Study Data of Each Patient in the Study Cohort (n = 20) Evaluated Concurrently with PDE Neo II and PTeye for Intraoperative Parathyroid Gland Identification

No	Disease	Age	Sex	BMI (kg/m^2)	Pre-operative USG	Pre-operative ^{99m}sestamibi	Procedure	Healthy/ diseased PG according to expert surgeon	PG histology	I or E	PG identification with NIRAF detection (Y/N)			Expert surgeon confidence before NIRAF imaging (visual exam)	Expert surgeon confidence after NIRAF imaging
											PDE Neo II		PTeye	Scale: 1 to 5 – low to high	
											In real-time? (Y/N)	Post hoc analysis? (Y/N)	In real-time? (Y/N)		
1	Graves' disease	59	M	27.3	N/A	N/A	TT	Healthy	Not available	I	Y	Y	Y	2	4
2	Primary hyper-parathyroidism	42	F	28.3	+	+	PT	Diseased	Hyper-cellular	E	Y	Y	Y	4	4.5
3	Papillary thyroid cancer	41	F	22.7	N/A	N/A	Completion TL	Healthy	Not available	I	Y	Y	Y	4.5	4.5
4	Benign multinodular goiter	59	F	35.1	N/A	N/A	Rt TL	Healthy	Not available	I	Y	Y	Y	3	4
5	Primary hyper-parathyroidism	52	F	23.5	N/A	N/A	PT	Healthy	Not available	I	Y	Y	Y	4	4.5
					N/A	N/A		Diseased	Normo-cellular	E	Y	Y	Y	4	4
					+	N/A		Diseased	Hyper-cellular	E	Y	Y	Y	4	4.5
6	Papillary thyroid cancer	30	M	41.7	N/A	N/A	Repeat CND and Rt MRND	None seen	Not available	-	-	-	-	-	-
7	Primary hyper-parathyroidism	64	F	26.0	+	+	PT	Diseased	Hyper-cellular	E	Y	Y	Y	3.5	3.5
					N/A	N/A		Healthy	Not available	I	Y	Y	Y	3.5	4
8	Papillary thyroid cancer	23	F	21.6	N/A	N/A	Rt TL	Healthy	Not available	I	Y	Y	Y	4.5	4.5
					N/A	N/A		Healthy	Not available	I	Y	Y	Y	4	4.5
9	Medullary	22	F	18.8	N/A	N/A	TT	Healthy	Not	I	N	N	Y	4	3

#	Diagnosis	Age	Sex	BMI			Surgery								
	thyroid cancer								available						
					N/A	N/A		Healthy	Not available	I	N	N	Y	3	2
					Same PG	Same PG		same PG ex vivo	Normo-cellular	E	N	N	Y	-	-
10	MEN2A with Hashimoto's thyroiditis	65	F	41.7	N/A	N/A	TT	Healthy	Not available	I	Y	Y	Y	4.5	5
					N/A	N/A		Healthy	Not available	I	Y	Y	Y	4.5	5
					N/A	N/A		Healthy	Not available	I	Y	Y	Y	3	3
11	Primary hyper-parathyroidism	59	F	28.9	+	N/A	PT	Diseased	Hyper-cellular	E	Y	Y	Y	4	4.5
12	Primary hyper-parathyroidism	81	M	21.5	+	N/A	PT	Diseased	Hyper-cellular	E	Y	Y	Y	4	4.5
13	Benign multinodular goiter	61	F	33.1	N/A	N/A	TT	Healthy	Not available	I	Y	Y	Y	4	4.5
					N/A	N/A		Healthy	Not available	I	Y	Y	Y	4	4.5
14	Papillary thyroid cancer with Hashimoto's thyroiditis	23	M	25.6	N/A	N/A	TT with CND and Rt MRND	Healthy	Not available	I	Y	N	Y	4	4.5
					N/A	N/A		Healthy	Not available	I	Y	N	Y	4	4.5
					N/A	N/A		Healthy	Not available	I	N	Y	N	4	3
15	Primary hyper-parathyroidism	68	F	39.0	+	N/A	PT	Diseased	Hyper-cellular	E	Y	Y	Y	4	4.5
16	Primary hyper-parathyroidism	58	F	26.4	N/A	N/A	PT	Healthy	Not available	I	Y	Y	Y	4	4.5
					+	+		Diseased		I	Y	N	Y	4	4.5
					Same PG	Same PG		same PG ex vivo	Hyper-cellular	E	Y	Y	Y	-	-
17	Multinodular goiter with Hashimoto's thyroiditis and primary hyper-parathyroidism	56	F	42.4	-	N/A	TT with PT	Diseased		I	Y	Y	Y	4	4.5
					Same PG	Same PG		same PG ex vivo	Hyper-cellular	E	Y	Y	Y	-	-
					-	N/A		Diseased		I	Y	Y	Y	4	4.5
					Same PG	Same PG		same PG ex vivo	Hyper-cellular	E	Y	Y	Y	-	-
18	Primary hyper-parathyroidism	82	F	32.2	+	-	PT	Diseased	Hyper-cellular	E	Y	N	Y	4	4.5
19	Medullary	67	F	27.0	N/A	N/A	TT	Healthy	Not	I	Y	Y	Y	4.5	4.5

No														
	thyroid cancer with Hashimoto's thyroiditis							available						
					N/A	N/A		Healthy	Not available	I	Y	Y	Y	4.5	4.5
					N/A	N/A		Healthy	Not available	I	Y	Y	Y	4.5	4.5
20	Benign multinodular goiter	61	F	29.9	N/A	N/A	Rt TL	Healthy	Not available	I	Y	Y	Y	4.5	4.5

CND, central neck dissection; E, ex vivo; I, in situ; Lt, left; MEN2A, multiple endocrine neoplasia 2A; MRND, modified radical neck dissection; NIRAF, near infrared autofluorescence; No, patient number; PG, parathyroid gland; PT, parathyroidectomy; Rt, right; TL, thyroid lobectomy; TT, total thyroidectomy; USG, ultrasonography.